THE JOURNAL OF PHYSICAL CHEMISTRY C

Article

pubs.acs.org/JPCC

Rigorous and Fast Discrete Dipole Approximation for Particles near a Plane Interface

Maxim A. Yurkin*[,†,‡] and Marcus Huntemann[§,∥]

[†]Voevodsky Institute of Chemical Kinetics and Combustion SB RAS, Institutskaya 3, Novosibirsk, 630090 Russia

[‡]Novosibirsk State University, Pirogova 2, Novosibirsk, 630090 Russia

[§]Institute of Environmental Physics, University of Bremen, Otto-Hahn-Allee 1, Bremen, 28359 Germany

[∥]Alfred Wegener Institute, Helmholtz Centre for Polar and Marine Research, Am Handelshafen 12, Bremerhaven, 27570 Germany

Supporting Information

ABSTRACT: The discrete dipole approximation (DDA) is a widely used method for simulation of various optical properties of nanoparticles of arbitrary shape and composition. We present a modification of the DDA to rigorously treat particles located above the plane homogeneous substrate. The modification is based on discretization of only the particle itself and retains the three-dimensional fast Fourier transform acceleration scheme of the free-space DDA; hence, it has the same order of computational complexity. It is implemented in the recent version of the open-source ADDA code, available for anyone to use. The method shows extremely good accuracy (better than 0.4%) in test simulations of far-field scattering for spheres and spheroids above transparent and metallic substrates, using the T-matrix method as a reference. An example of near-field calculation is presented for a silver sphere on a glass substrate.

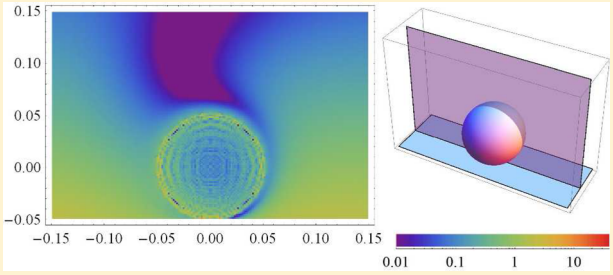

INTRODUCTION

Theoretical simulations of optical properties of nanoparticles have become an indispensable part of nanoscience. Among various existing methods[1,2] the discrete dipole approximation (DDA) is a frequency-domain volume-discretization method to simulate the interaction of electromagnetic waves with particles of arbitrary shape and composition.[3−5] Although the original applications of the DDA were related to cosmic dust and atmospheric aerosols,[3,4] the last 2 decades witnessed its wide application to nanoparticles, mostly plasmonic ones, starting from the works of Schatz and co-workers.[6,7] Those applications presented certain numerical challenges,[8,9] but also led to extension of the DDA to new physical phenomena. The latter include surface-enhanced Raman scattering (SERS),[6] metal-enhanced fluorescence,[10,11] electron-energy-loss spectroscopy,[12−14] cathodoluminescence,[15,16] near-field radiative transfer,[17,18] nonlinear absorption,[19] and scattering of short pulses.[20,21] The main advantage of the DDA is its conceptual simplicity combined with relatively good computational efficiency. The latter is determined by the solution of the large system of linear equations, which is performed by the conjugate-gradient iterative solver with matrix-vector product computed using the fast Fourier transform (FFT) on a regular grid.[22] Although historically the DDA contains "approximation" in its name, it is a direct consequence of Maxwell's equations[5] and, hence, is a "numerically exact" method;[23] that is, it reaches any specified accuracy for any problem given sufficient computational resources. Moreover, wide use of the DDA is facilitated by a number of available open-source codes.[4,13,14,24,25]

While the DDA is mostly applied to finite particles in a homogeneous medium, there are a multitude of applications, where a particle is located near a plane surface (substrate). The rigorous extension of the DDA (or similar methods) to such problems is possible[10,17,25−30] but introduces two additional issues. The first one is the technical difficulty of calculation of interaction of two dipoles near the substrate, related to the so-called Sommerfeld integrals.[31] Efficient evaluation of such integrals is still a field of active research.[32,33] However, there exist reliable routines,[31] which were used in previous DDA implementations.[25−27] The second issue is the lack of the translational symmetry of the dipole−dipole interaction (Green's tensor), which breaks the above-mentioned three-dimensional (3D)-FFT acceleration. As a result, existing DDA implementations either do not use FFT at all[25] or use only two-dimensional (2D) FFT due to the remaining translational symmetry parallel to the surface.[27] The computational complexity of the method is then $O(N_{iter}N^2)$ or $O(N_{iter}N^{4/3} \log N)$, respectively, where N is the number of dipoles (volume elements) in particle discretization and N_{iter} is the number of iterations required for the convergence of the iterative solver (typically, $N_{iter} \ll N$). A 3D-FFT acceleration for such cases

Received: September 23, 2015
Revised: November 26, 2015
Published: November 30, 2015

DOI: 10.1021/acs.jpcc.5b09271
J. Phys. Chem. C 2015, 119, 29088−29094

with complexity $O(N_{iter}N \log N)$, same as for the free-space DDA, was mentioned for similar volume-integral equation methods,[29,34] but has never been implemented in a DDA code. While this difference in computational time may seem purely technical, it quickly becomes prohibitive for large N. For instance, when $N > 10^6$, as typically required for satisfactory accuracy in plasmonic nanoparticles,[8] the difference between the 2D- and 3D-FFT schemes is more than 100 times.

Those issues explain why the DDA has been used rarely for particles on substrate and mostly in combination with different approximations. First to mention is the so-called image approximation: that is, the exact surface-induced part of Green's tensor is approximated by interaction with an image dipole (see eq 7 below).[6,13,35] While this approximation is exact in the static case (all characteristic geometric lengths are much smaller than the wavelength) or when the substrate is a perfect reflector, it is almost impossible to quantify the error for a particular nanoparticle a priori.[26] Moreover, no FFT acceleration has been reported in combination with this approach. A second, even less accurate approximation (never exact), is that of replacing the substrate by a homogeneous medium with an effective refractive index.[36−38] Finally, the third approximation is based on brute-force discretization of a block of substrate.[7,39−42] It allows one to easily consider multilayered or inhomogeneous substrate[40] and to use standard free-space DDA codes, but requires much longer simulation time and additional consideration of hard-to-control convergence with respect to the block size.

In this paper we present a way to retain 3D-FFT acceleration in the DDA with rigorous consideration of particle-substrate configuration (discretizing only the particle), and describe the details of its efficient implementation in the open-source ADDA code,[24] which supports parallelization on modern hardware. We performed test simulations for spheres and spheroids and verify the results of far-field scattering against that of the T-matrix method. An example of near-field computations is also presented. A preliminary version of these results was presented previously as a conference talk.[43]

THEORY

DDA Basics. The DDA is based on the discretization of the volume-integral electric-field equation, where each of the volume elements can be considered a dipole.[5] Generalizing the DDA to particles near a surface boils down to replacing the free-space Green's tensor $\overline{\mathbf{G}}$ by $\overline{\mathbf{G}} + \overline{\mathbf{R}}$, where $\overline{\mathbf{R}}$ is the "reflected" (surface-induced) part. Here, we limit ourselves to nonmagnetic isotropic materials and particles completely above the substrate, but discuss possible generalizations below. The main DDA equations[5] then become (see Supporting Information for details)

$$\overline{\boldsymbol{\alpha}}_i^{-1}\mathbf{P}_i - \sum_j (\overline{\mathbf{G}}_{ij} + \overline{\mathbf{R}}_{ij})\mathbf{P}_j = \mathbf{E}_i^{\mathrm{inc}} \tag{1}$$

where $\overline{\boldsymbol{\alpha}}_i$ and $\mathbf{P}_i$ are the polarizability and total polarization of the dipole i, respectively, and $\mathbf{E}_i^{\mathrm{inc}}$ is the incident field at dipole position $\mathbf{r}_i$. The latter field is in the presence of substrate, that is, it is either a sum of incoming (if no surface is present, e.g. a plane wave) and reflected or a transmitted one, depending on the direction of propagation of the incoming field (Supporting Information, eqs S14−S16). Moreover, we postulate $\overline{\mathbf{G}}_{ii} \equiv \overline{\mathbf{0}}$, that is, the proper treatment of the corresponding singularity is traditionally included in the expression for $\overline{\boldsymbol{\alpha}}_i$ (see Supporting Information, eq S12). To determine the unknown vector $\mathbf{P}$, system of linear eq 1 is solved by an iterative solver. Then the main computational bottleneck is evaluation of the matrix−vector products (the sum in eq 1). The key for handling this bottleneck is transforming the sum into a convolution that is further evaluated with the FFT. In the following we describe this procedure separately for the tensors $\overline{\mathbf{G}}$ and $\overline{\mathbf{R}}$.

Evaluation of the Direct-Interaction Part. The first part of the sum in eq 1 is the same as that in the free-space DDA.[5] We briefly repeat its evaluation here as an introduction to the subsequent evaluation of the reflected part. The main ingredient is the following translational symmetry,

$$\overline{\mathbf{G}}_{ij} = \overline{\mathbf{G}}(\mathbf{r}_i, \mathbf{r}_j) = \overline{\mathbf{G}}(\mathbf{r}_i - \mathbf{r}_j) \equiv \overline{\mathbf{G}}'_{\mathbf{i}-\mathbf{j}} \tag{2}$$

where we assumed that dipoles are located on a uniform cubical grid and $\mathbf{i}$, $\mathbf{j}$ are vector indices. $\overline{\mathbf{G}}'_{\mathbf{i}} \equiv \overline{\mathbf{G}}_{\mathbf{i}0} = \overline{\mathbf{G}}(\mathbf{i}d)$ for $|i_\mu| \le N_\mu$ ($\overline{\mathbf{G}}'_{\mathbf{0}} \equiv \overline{\mathbf{0}}$) and $\overline{\mathbf{G}}'_{\mathbf{i}}$ is assumed periodic with period $2N_\mu$ along the axis μ (d is the dipole spacing and N_μ is the size of the dipole grid). Then the sum is transformed into a discrete convolution,

$$\sum_{j=1}^{N} \overline{\mathbf{G}}_{ij}\mathbf{P}_j = \sum_{\mathbf{j}=(1,1,1)}^{(N_x,N_y,N_z)} \overline{\mathbf{G}}'_{\mathbf{i}-\mathbf{j}}\mathbf{P}_{\mathbf{j}} = \sum_{\mathbf{j}=(1,1,1)}^{(2N_x,2N_y,2N_z)} \overline{\mathbf{G}}'_{\mathbf{i}-\mathbf{j}}\mathbf{P}'_{\mathbf{j}} \tag{3}$$

where $\mathbf{P}'$ is the periodic (same as $\overline{\mathbf{G}}'$) zero-padded extension of $\mathbf{P}$:

$$\mathbf{P}'_{\mathbf{j}} = \begin{cases} \mathbf{P}_{\mathbf{j}}, \ \forall\ \mu\colon 1 \le j_\mu \le N_\mu; \\ \mathbf{0}, \text{ otherwise.} \end{cases} \tag{4}$$

Finally, the convolution is evaluated using the Fourier calculus as

$$[\overline{\mathbf{G}}_{ij}]\mathbf{P} = F^{-1}(F(\overline{\mathbf{G}}')F(\mathbf{P}')) \tag{5}$$

where F and F^{-1} are the direct and inverse discrete Fourier transforms applied to each component of the vector or tensor, independently, and $[\overline{\mathbf{G}}_{ij}]$ denotes the matrix built up by varying indices i and j.

Evaluation of the Substrate-Induced Interaction. We define the surface to be aligned with the horizontal plane ($z = -h_s$) at distance h_s below the origin; the latter is traditionally placed in the particle center. Then the reflected part is a function of the distance between the evaluation point and the image of source:

$$\overline{\mathbf{R}}(\mathbf{r}, \mathbf{r}') = \overline{\mathbf{R}}(x - x', y - y', z + z' + 2h_s) = \overline{\mathbf{R}}(\boldsymbol{\rho}, Z) \tag{6}$$

where $\boldsymbol{\rho}$ and Z are the components of the distance parallel and perpendicular to the surface, respectively. The simplest approximation to $\overline{\mathbf{R}}$ is that of a single image dipole,

$$\overline{\mathbf{R}}_{\mathrm{im}}(\boldsymbol{\rho}, Z) = \frac{1 - \varepsilon_s}{1 + \varepsilon_s}\overline{\mathbf{G}}(\boldsymbol{\rho}, Z)(\overline{\mathbf{I}} - 2\overline{\mathbf{I}}_z) \tag{7}$$

where $\overline{\mathbf{I}}_z = \hat{\mathbf{e}}_z\hat{\mathbf{e}}_z$ is a projector on the z-axis, $\mathbf{e}_z$ is the unit vector along the z-axis, and ε_s is the complex electric permittivity of the substrate. Here and further on, we use carets above two vectors (not necessarily unit ones) to denote a dyadic constructed from them. The accuracy of the image-dipole approximation improves with increasing Z and/or $|\varepsilon_s|$. By contrast, the rigorous expression for the reflected term is

DOI: 10.1021/acs.jpcc.5b09271
J. Phys. Chem. C 2015, 119, 29088−29094

$$\bar{\mathbf{R}}(\boldsymbol{\rho}, Z) = \frac{\hat{\rho}\hat{\rho}}{\rho^2}(I_\rho^{\mathrm{H}} + I_\varphi^{\mathrm{H}}) - (\bar{\mathbf{I}} - \bar{\mathbf{I}}_z)I_\varphi^{\mathrm{H}} + \frac{\hat{\rho}\hat{e}_z - \hat{e}_z\hat{\rho}}{\rho} I_\rho^{\mathrm{V}} + \bar{\mathbf{I}}_z I_z^{\mathrm{V}} + \bar{\mathbf{R}}_{\mathrm{im}}(\boldsymbol{\rho}, Z) \quad (8)$$

where I_ρ^{H}, I_φ^{H}, I_ρ^{V}, and I_z^{V} are the Sommerfeld integrals[31] that depend on ρ, Z, and ε_s.

To exploit the specific symmetry over the z-axis in eq 6, we define the auxiliary vector [cf. eq 2]

$$\bar{\mathbf{R}}'_{\mathbf{i}} = \bar{\mathbf{R}}_{\mathbf{i}\{0,0,0\}} = \bar{\mathbf{R}}(i_x d, i_y d, i_z d + 2h_1) \quad (9)$$

for $|i_{x,y}| \le N_{x,y}$, $0 \le i_z < 2N_z - 1$. Additionally, $\bar{\mathbf{R}}'_{\mathbf{i}} \equiv 0$ for $i_z = 2N_z - 1$ and is further extended periodically (same as $\bar{\mathbf{G}}'$). h_1 is the distance from the lowest dipole layer (dipole centers) to the surface. The sum over the z-axis is now a discrete *correlation*, which can be transformed into a convolution by inverting the order of z-components of $\mathbf{P}$,

$$\sum_{j=1}^{N} \bar{\mathbf{R}}_{ij}\mathbf{P}_j = \sum_{\mathbf{j}=(1,1,1)}^{(2N_x,2N_y,2N_z)} \bar{\mathbf{R}}'_{\mathbf{i}-\mathbf{j}}\tilde{\mathbf{P}}_{\mathbf{j}} \quad (10)$$

where

$$\tilde{\mathbf{P}}_{\mathbf{j}} = \begin{cases} \mathbf{P}_{\{j_x,j_y,1\}}, & 1 \le j_{x,y} \le N_{x,y} \text{ and } j_z = 1; \\ \mathbf{P}_{\{j_x,j_y,2N_z+2-j_z\}}, & 1 \le j_{x,y} \le N_{x,y} \\ & \quad \text{and } N_z < j_z \le 2N_z; \\ \mathbf{0}, & \text{otherwise.} \end{cases} \quad (11)$$

Conveniently, $\tilde{\mathbf{P}}$ satisfies

$$F(\tilde{\mathbf{P}}) = F_z^{-1}F_yF_x(\mathbf{P}') \quad (12)$$

where F_μ is the 1D discrete Fourier transform along the axis μ. Combining eqs 5, 10, and 12, we finally obtain the main result of this paper:

$$[\bar{\mathbf{G}}_{ij} + \bar{\mathbf{R}}_{ij}]\mathbf{P} = F^{-1}((F(\bar{\mathbf{G}}')F_z + F(\bar{\mathbf{R}}')F_z^{-1})F_xF_y(\mathbf{P}')) \quad (13)$$

Since $F(\bar{\mathbf{G}}')$ and $F(\bar{\mathbf{R}}')$ need to be calculated only once, the computational time for matrix–vector product is only slightly (by approximately 30% if $N_x = N_y = N_z$) larger than that for the free-space DDA. In particular, it has the same complexity order $O(N \log N)$.

Scattered Fields. Certain changes in the formulas to calculate the scattered fields (based on the determined $\mathbf{P}$) are also required, but they are straightforward and are discussed in the Supporting Information (eqs S20–S22). These fields are commonly represented through the amplitude or Mueller scattering matrices, which are independent of the distance to a detector and describe all states of incident and scattered polarizations.[44] However, generalization of these concepts to the cases when either incoming or scattered field is in the substrate has not been discussed in the literature. Therefore, we propose such a generalization and describe it in detail in the Supporting Information (eqs S28–S29). In particular, if we consider scattering into a substrate only for nonabsorbing one, the Mueller matrix, relating the incoming (in) and scattered (sca) Stokes vectors, is defined as

$$\begin{pmatrix} I_{\mathrm{sca}} \\ Q_{\mathrm{sca}} \\ U_{\mathrm{sca}} \\ V_{\mathrm{sca}} \end{pmatrix} = \frac{1}{k_{\mathrm{sca}}^2 r^2} \begin{pmatrix} S_{11} & S_{12} & S_{13} & S_{14} \\ S_{21} & S_{22} & S_{23} & S_{24} \\ S_{31} & S_{32} & S_{33} & S_{34} \\ S_{41} & S_{42} & S_{43} & S_{44} \end{pmatrix} \begin{pmatrix} I_{\mathrm{in}} \\ Q_{\mathrm{in}} \\ U_{\mathrm{in}} \\ V_{\mathrm{in}} \end{pmatrix} \quad (14)$$

where k_{sca} is the wave vector for the scattering direction (always real), r is the distance to the detector, and we assume the standard textbook definitions of the Stokes vector through the electric fields,[45] which contain the real part of the medium refractive index.

SOFTWARE IMPLEMENTATION

The developed approach has been implemented in the open-source code ADDA. In particular, these algorithms are included in the version 1.3b4, available online.[46] Moreover, they are fully integrated with other parts of ADDA, including employed parallelization technologies. In particular, MPI parallelization allows solving huge problems (up to 1 billion dipoles[24]) using a large computer cluster. OpenCL mode allows significant acceleration for moderately sized problems using a modern video card (GPU).[47] These features also distinguish current implementation from existing alternatives, described in the Introduction. Details of the implementation are described in the manual.[48] Of special interest is the capability to calculate the decay-rate enhancement for a point emitter near nanoparticles of arbitrary shape,[11,49,50] which is relevant for rigorous treatment of SERS and metal-enhanced fluorescence. Now such simulations can be easily performed above the plane substrate.

RESULTS AND DISCUSSION

In the following we consider three test cases. The first one corresponds to Figure 4.10 of ref 51—a silver sphere (radius R = 50 nm, refractive index 0.25 + 3.14i) placed on a glass substrate (m_s = 1.5), illuminated by a plane wave propagating from below at 60° relative to the surface normal (evanescent illumination, see inset in Figure 1a). The wavelength is 488 nm, and ADDA v.1.3b4 was used with two levels of discretization (64 and 128 dipoles per sphere diameter, which is equivalent to N_x defined above). To further improve the accuracy, we employed an empirical linear extrapolation (to zero dipole size): $f(\mathrm{extrap}) = 2f(N_x = 128) - f(N_x = 64)$ for any computed value f, for example, for the intensity scattered at a specific angle. This approach is a simplified version of a previously studied quadratic extrapolation;[52] however, in this paper we postulate it as it is and judge it purely by its results below. Figure 1 shows perpendicular and parallel scattering intensities ($I_{\mathrm{per}} = S_{11} - S_{12}$ and $I_{\mathrm{par}} = S_{11} + S_{12}$, respectively) in the main scattering plane in comparison with the reference T-matrix results. The latter were calculated using NFM-DS 1.1[53] and renormalized to the definition of eq 14.

Second test case is the same as the first one, but for the above-substrate illumination (also 60° relative to the surface normal)—corresponding results are shown in Figure 2. For both test cases the DDA accuracy is good and smoothly decreases with refining discretization, which explains even better accuracy of the extrapolation results. We had to use relatively fine discretization to obtain such high accuracy, which is not surprising for metallic nanoparticles.[8] Still, the computational speed is perfectly suitable for large-scale applications, thanks to the efficient 3D-FFT implementation. The DDA simulation for N_x = 64 took only 5 min on a single core of a

DOI: 10.1021/acs.jpcc.5b09271
J. Phys. Chem. C 2015, 119, 29088–29094

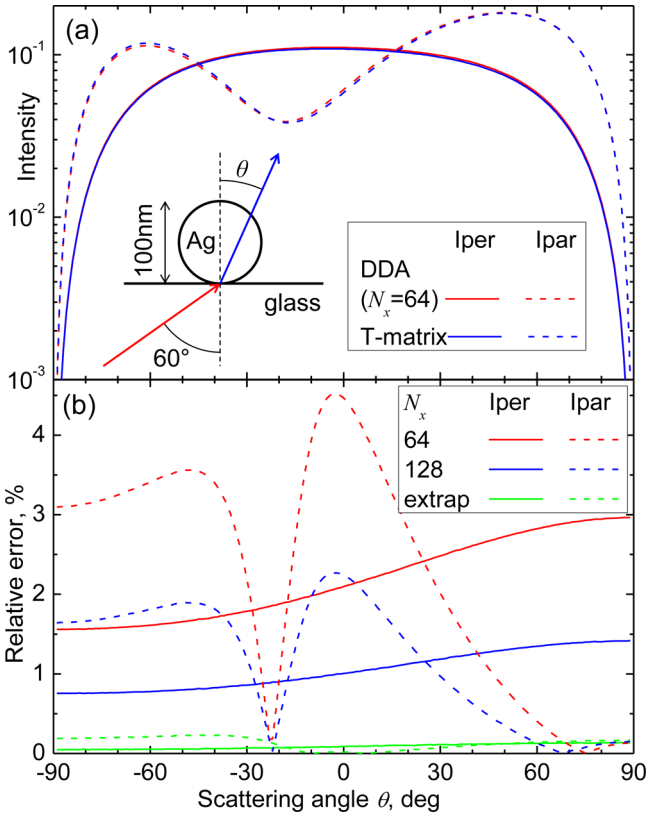

Figure 1. Perpendicular and parallel scattering intensities for a Ag sphere on a glass substrate, illuminated by a plane wave from the substrate in evanescent configuration. DDA simulations are compared with the reference T-matrix results. (a) Direct assessment of N_x = 64 DDA results in a logarithmic scale (other DDA variants are not shown for clarity). (b) Relative differences between the three DDA variants, including the linearly extrapolated one, and the reference.

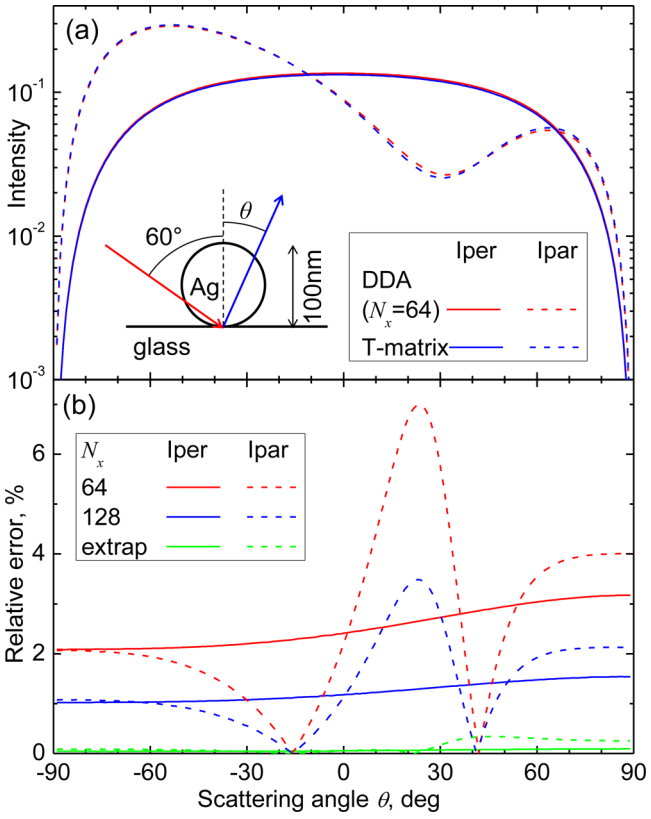

Figure 2. Same as Figure 1, but for the above-substrate illumination.

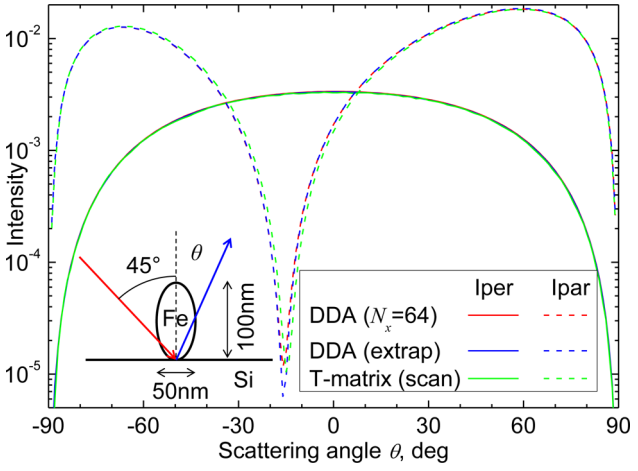

Figure 3. Perpendicular and parallel scattering intensities (in a logarithmic scale) for a Fe spheroid on a Si substrate, illuminated by a plane wave, computed with the DDA and the T-matrix method. The latter data has been digitized from ref 51 and scaled.

laptop processor (Intel Core i7-2630QM), while the extrapolated results with relative accuracy better than 0.4% were obtained within 1 h.

The third test case corresponds to Figure 4.7 of ref 51—an iron oblate spheroid (semiaxes 25, 25, and 50 nm, refractive index 1.35 + 1.97i) placed on silicon substrate (m_s = 4.37 + 0.08i), illuminated by a plane wave with wavelength of 488 nm propagating from above at 45° relative to the surface normal (see inset in Figure 3). In this case the reference T-matrix results are obtained by digitizing Figure 4.7 of ref 51, which is expected to have worse accuracy than those used in the first two cases. Moreover, the absolute magnitude of those results is unknown, so we scaled them to have the same maximum value as the extrapolated DDA (for each curve). The comparison of DDA results (N_x = 64 and extrapolated one) with this T-matrix data is given in Figure 3. The agreement for perpendicular scattering intensity is within 4% for values larger than 10^{-4}, which is perfect given the digitization in a logarithmic scale. There is a certain disagreement for parallel scattering intensity near its minimum, but it may well be due to uncertainty of the original T-matrix result. In particular, the comparison of the latter with the discrete sources method[51] showed differences comparable to that in Figure 3.

Finally, we provide an example of near-field calculation for configuration of the first test case (see Figure 1a). For that we considered a 300 × 100 × 200 nm box around the sphere (Figure 4) and filled it (except the sphere) with virtual dipoles with refractive index of 1.00001 (corresponding to almost vacuum). The dipole size is the same as that for N_x = 64 discretization of the original sphere. Then the solution of the DDA problem for the whole box automatically provides the field inside it, which, in turn, is internal and near-field for the original sphere. While this workaround is not as efficient as specialized routines for the free-space DDA,[54] it also benefits from the 3D-FFT acceleration and has computational time of the same order of magnitude (35 min on the same processor). In particular, it is much faster than the direct evaluation of near fields from the determined **P** independently for each probe

DOI: 10.1021/acs.jpcc.5b09271
J. Phys. Chem. C 2015, 119, 29088−29094

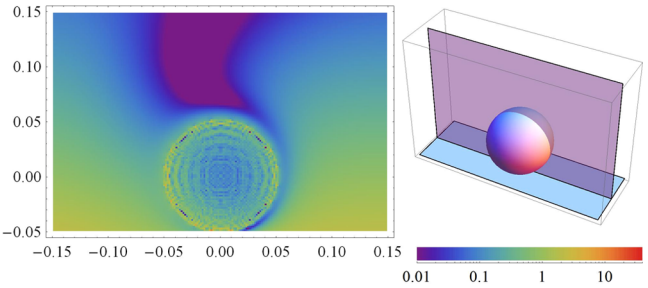

Figure 4. DDA simulations of the field intensity ($|\mathbf{E}|^2$) in a logarithmic scale near and inside a Ag sphere on a glass substrate, illuminated by a plane wave of unit amplitude from the substrate in evanescent configuration (same as in Figure 1, incident polarization along the *y*-axis). Shown is the central cross section (*xz*-plane); the axis labels are in units of μm.

point, which requires computation of sums similar to the one in eq 1 and has $O(N^2)$ complexity. Figure 4 shows the intensity of these fields in the central cross section through the sphere. All cross sections through the box are presented as an animation in the Supporting Information. As expected, far from the sphere the field follows an exponential decay of the evanescent wave along the *z*-axis. The maximum field values occur near the boundary of the sphere, although the values are not that large due to the nonresonance wavelength.

CONCLUSIONS

We presented a reliable, fast, open-source, and easy-to-use tool to simulate interaction of electromagnetic fields with particles of arbitrary shape and composition located on or near a semi-infinite plane substrate. In particular, only the particle itself needs to be discretized and the simulation time is only slightly larger than that when no substrate is present. Several simulation examples prove the correctness of the implementation and demonstrate high accuracy. However, a systematic accuracy study, similar to those performed for the free-space DDA,[8,55,56] is yet outstanding and an important topic for future research.

The tests were performed only for isotropic particles, but anisotropic ones with diagonal refractive-index tensor can also be handled by the existing code. However, anisotropic substrate is much more complicated to handle since it breaks some of the symmetry, and hence the FFT acceleration. It is also possible to consider particles wholly inside the nonabsorbing substrate by dividing all refractive indices (and the wavelength) by that of the substrate. We believe this tool may find many applications in nanoscience and other fields, for example, for simulation of optical properties of biological particles absorbed on a substrate and of large dust particles with surface roughness.

Further ideas for development of the approach presented here includes particles inside an absorbing substrate, or near a multilayered substrate—both require only the calculation of a different tensor $\bar{\mathbf{R}}(\boldsymbol{\rho}, Z)$. Consideration of a particle intersecting with the surface, or more generally, a multiparticle configuration placed in different media, would require a separate consideration of interaction between different parts. Some of them will have the same symmetry as in eq 6, others as in eq 2. Therefore, the order of computational complexity, corresponding to 3D-FFT, can be retained.

ASSOCIATED CONTENT

Supporting Information

The Supporting Information is available free of charge on the ACS Publications website at DOI: 10.1021/acs.jpcc.5b09271.

Derivation of eq 1 from the integral equation for the electric field; formulas for the incident field of incoming plane wave and for calculation of scattered fields and cross sections; generalization of definitions of amplitude and scattering matrices (PDF)

Animation of simulated near fields for the silver sphere on the glass substrate (AVI)

AUTHOR INFORMATION

Corresponding Author

*E-mail: yurkin@gmail.com.

Notes

The authors declare no competing financial interest.

ACKNOWLEDGMENTS

This work was partly supported by Russian Science Foundation (Grant No. 14-15-00155). We thank Vladimir Schmidt for providing reference T-matrix results, used in Figures 1 and 2. We are also grateful to the two anonymous reviewers for their constructive comments.

REFERENCES

(1) Karamehmedovic, M.; Schuh, R.; Schmidt, V.; Wriedt, T.; Matyssek, C.; Hergert, W.; Stalmashonak, A.; Seifert, G.; Stranik, O. Comparison of Numerical Methods in near-Field Computation for Metallic Nanoparticles. *Opt. Express* **2011**, *19*, 8939−8953.

(2) Coronado, E. A.; Encina, E. R.; Stefani, F. D. Optical Properties of Metallic Nanoparticles: Manipulating Light, Heat and Forces at the Nanoscale. *Nanoscale* **2011**, *3*, 4042−4059.

(3) Purcell, E. M.; Pennypacker, C. R. Scattering and Adsorption of Light by Nonspherical Dielectric Grains. *Astrophys. J.* **1973**, *186*, 705−714.

(4) Draine, B. T.; Flatau, P. J. Discrete-Dipole Approximation for Scattering Calculations. *J. Opt. Soc. Am. A* **1994**, *11*, 1491−1499.

(5) Yurkin, M. A.; Hoekstra, A. G. The Discrete Dipole Approximation: An Overview and Recent Developments. *J. Quant. Spectrosc. Radiat. Transfer* **2007**, *106*, 558−589.

(6) Yang, W. H.; Schatz, G. C.; Vanduyne, R. P. Discrete Dipole Approximation for Calculating Extinction and Raman Intensities for Small Particles with Arbitrary Shapes. *J. Chem. Phys.* **1995**, *103*, 869−875.

(7) Kelly, K. L.; Coronado, E.; Zhao, L.; Schatz, G. C. The Optical Properties of Metal Nanoparticles: The Influence of Size, Shape, and Dielectric Environment. *J. Phys. Chem. B* **2003**, *107*, 668−677.

(8) Yurkin, M. A.; de Kanter, D.; Hoekstra, A. G. Accuracy of the Discrete Dipole Approximation for Simulation of Optical Properties of Gold Nanoparticles. *J. Nanophotonics* **2010**, *4*, 041585.

(9) Yurkin, M. A. Computational Approaches for Plasmonics. In *Handbook of Molecular Plasmonics*; Della Sala, F., D'Agostino, S., Eds.; Pan Stanford Publishing: Singapore, 2013; pp 83−135.

(10) Rahmani, A.; Chaumet, P. C.; de Fornel, F. Environment-Induced Modification of Spontaneous Emission: Single-Molecule near-Field Probe. *Phys. Rev. A: At., Mol., Opt. Phys.* **2001**, *63*, 023819.

(11) D'Agostino, S.; Della Sala, F.; Andreani, L. C. Dipole-Excited Surface Plasmons in Metallic Nanoparticles: Engineering Decay Dynamics within the Discrete-Dipole Approximation. *Phys. Rev. B: Condens. Matter Mater. Phys.* **2013**, *87*, 205413.

(12) Henrard, L.; Lambin, P. Calculation of the Energy Loss for an Electron Passing near Giant Fullerenes. *J. Phys. B: At., Mol. Opt. Phys.* **1996**, *29*, 5127.

DOI: 10.1021/acs.jpcc.5b09271
J. Phys. Chem. C 2015, 119, 29088−29094

(13) Geuquet, N.; Henrard, L. EELS and Optical Response of a Noble Metal Nanoparticle in the Frame of a Discrete Dipole Approximation. *Ultramicroscopy* **2010**, *110*, 1075−1080.
(14) Bigelow, N. W.; Vaschillo, A.; Iberi, V.; Camden, J. P.; Masiello, D. J. Characterization of the Electron- and Photon-Driven Plasmonic Excitations of Metal Nanorods. *ACS Nano* **2012**, *6*, 7497−7504.
(15) Myroshnychenko, V.; Nelayah, J.; Adamo, G.; Geuquet, N.; Rodríguez-Fernández, J.; Pastoriza-Santos, I.; MacDonald, K. F.; Henrard, L.; Liz-Marzán, L. M.; Zheludev, N. I.; et al. Plasmon Spectroscopy and Imaging of Individual Gold Nanodecahedra: A Combined Optical Microscopy, Cathodoluminescence, and Electron Energy-Loss Spectroscopy Study. *Nano Lett.* **2012**, *12*, 4172−4180.
(16) Bigelow, N. W.; Vaschillo, A.; Camden, J. P.; Masiello, D. J. Signatures of Fano Interferences in the Electron Energy Loss Spectroscopy and Cathodoluminescence of Symmetry-Broken Nanorod Dimers. *ACS Nano* **2013**, *7*, 4511−4519.
(17) Baffou, G.; Quidant, R.; Girard, C. Thermoplasmonics Modeling: A Green's Function Approach. *Phys. Rev. B: Condens. Matter Mater. Phys.* **2010**, *82*, 165424.
(18) Edalatpour, S.; Francoeur, M. The Thermal Discrete Dipole Approximation (T-DDA) for near-Field Radiative Heat Transfer Simulations in Three-Dimensional Arbitrary Geometries. *J. Quant. Spectrosc. Radiat. Transfer* **2014**, *133*, 364−373.
(19) Dhoni, M. S.; Ji, W. Extension of Discrete-Dipole Approximation Model to Compute Nonlinear Absorption in Gold Nanostructures. *J. Phys. Chem. C* **2011**, *115*, 20359−20366.
(20) Chaumet, P. C.; Belkebir, K.; Rahmani, A. Coupled-Dipole Method in Time Domain. *Opt. Express* **2008**, *16*, 20157−20165.
(21) Kim, K.-H.; Yurkin, M. A. Time-Domain Discrete-Dipole Approximation for Simulation of Temporal Response of Plasmonic Nanoparticles. *Opt. Express* **2015**, *23*, 15555−15564.
(22) Goodman, J. J.; Draine, B. T.; Flatau, P. J. Application of Fast-Fourier-Transform Techniques to the Discrete-Dipole Approximation. *Opt. Lett.* **1991**, *16*, 1198−1200.
(23) Mishchenko, M. I.; Tishkovets, V. P.; Travis, L. D.; Cairns, B.; Dlugach, J. M.; Liu, L.; Rosenbush, V. K.; Kiselev, N. N. Electromagnetic Scattering by a Morphologically Complex Object: Fundamental Concepts and Common Misconceptions. *J. Quant. Spectrosc. Radiat. Transfer* **2011**, *112*, 671−692.
(24) Yurkin, M. A.; Hoekstra, A. G. The Discrete-Dipole-Approximation Code ADDA: Capabilities and Known Limitations. *J. Quant. Spectrosc. Radiat. Transfer* **2011**, *112*, 2234−2247.
(25) Loke, V. L. Y.; Mengüç, M. P.; Nieminen, T. A. Discrete Dipole Approximation with Surface Interaction: Computational Toolbox for MATLAB. *J. Quant. Spectrosc. Radiat. Transfer* **2011**, *112*, 1711−1725.
(26) Taubenblatt, M. A.; Tran, T. K. Calculation of Light-Scattering from Particles and Structures on a Surface by the Coupled-Dipole Method. *J. Opt. Soc. Am. A* **1993**, *10*, 912−919.
(27) Schmehl, R.; Nebeker, B. M.; Hirleman, E. D. Discrete-Dipole Approximation for Scattering by Features on Surfaces by Means of a Two-Dimensional Fast Fourier Transform Technique. *J. Opt. Soc. Am. A* **1997**, *14*, 3026−3036.
(28) Girard, C. Near Fields in Nanostructures. *Rep. Prog. Phys.* **2005**, *68*, 1883.
(29) Søndergaard, T. Modeling of Plasmonic Nanostructures: Green's Function Integral Equation Methods. *Phys. Status Solidi B* **2007**, *244*, 3448−3462.
(30) Campione, S.; Guclu, C.; Ragan, R.; Capolino, F. Enhanced Magnetic and Electric Fields via Fano Resonances in Metasurfaces of Circular Clusters of Plasmonic Nanoparticles. *ACS Photonics* **2014**, *1*, 254−260.
(31) Lager, D. L.; Lytle, R. J. *Fortran Subroutines for the Numerical Evaluation of Sommerfeld Integrals Unter Anderem*; Technical Report UCRL-51821; Lawrence Livermore National Laboratory: Livermore, CA, 1975.
(32) Panasyuk, G. Y.; Schotland, J. C.; Markel, V. A. Short-Distance Expansion for the Electromagnetic Half-Space Green's Tensor: General Results and an Application to Radiative Lifetime Computations. *J. Phys. A: Math. Theor.* **2009**, *42*, 275203.
(33) Mackowski, D. W. A Generalization of Image Theory to Predict the Interaction of Multipole Fields with Plane Surfaces. *J. Quant. Spectrosc. Radiat. Transfer* **2010**, *111*, 802−809.
(34) Eremin, Y. A.; Ivakhnenko, V. I. Modeling of Light Scattering by Non-Spherical Inhomogeneous Particles. *J. Quant. Spectrosc. Radiat. Transfer* **1998**, *60*, 475−482.
(35) Prieto, M.; Arenal, R.; Henrard, L.; Gomez, L.; Sebastian, V.; Arruebo, M. Morphological Tunability of the Plasmonic Response: From Hollow Gold Nanoparticles to Gold Nanorings. *J. Phys. Chem. C* **2014**, *118*, 28804−28811.
(36) Guler, U.; Turan, R. Effect of Particle Properties and Light Polarization on the Plasmonic Resonances in Metallic Nanoparticles. *Opt. Express* **2010**, *18*, 17322−17338.
(37) Kessentini, S.; Barchiesi, D.; D'Andrea, C.; Toma, A.; Guillot, N.; Di Fabrizio, E.; Fazio, B.; Maragó, O. M.; Gucciardi, P. G.; Lamy de la Chapelle, M. Gold Dimer Nanoantenna with Slanted Gap for Tunable LSPR and Improved SERS. *J. Phys. Chem. C* **2014**, *118*, 3209−3219.
(38) Dodson, S. L.; Cao, C.; Zaribafzadeh, H.; Li, S.; Xiong, Q. Engineering Plasmonic Nanorod Arrays for Colon Cancer Marker Detection. *Biosens. Bioelectron.* **2015**, *63*, 472−477.
(39) Malinsky, M. D.; Kelly, K. L.; Schatz, G. C.; Van Duyne, R. P. Nanosphere Lithography: Effect of Substrate on the Localized Surface Plasmon Resonance Spectrum of Silver Nanoparticles. *J. Phys. Chem. B* **2001**, *105*, 2343−2350.
(40) D'Agostino, S.; Pompa, P. P.; Chiuri, R.; Phaneuf, R. J.; Britti, D. G.; Rinaldi, R.; Cingolani, R.; Della Sala, F. Enhanced Fluorescence by Metal Nanospheres on Metal Substrates. *Opt. Lett.* **2009**, *34*, 2381−2383.
(41) Perassi, E. M.; Hrelescu, C.; Wisnet, A.; Döblinger, M.; Scheu, C.; Jäckel, F.; Coronado, E. A.; Feldmann, J. Quantitative Understanding of the Optical Properties of a Single, Complex-Shaped Gold Nanoparticle from Experiment and Theory. *ACS Nano* **2014**, *8*, 4395−4402.
(42) Ren, S.; Wang, B.; Zhang, H.; Ding, P.; Wang, Q. Sandwiched ZnO@Au@Cu2O Nanorod Films as Efficient Visible-Light-Driven Plasmonic Photocatalysts. *ACS Appl. Mater. Interfaces* **2015**, *7*, 4066−4074.
(43) Yurkin, M. A.; Huntemann, M. *Discrete Dipole Approximation for Particles near Surface: A 3D-FFT-Accelerated Implementation*. In *Proceedings of 10th International Conference on Laser-light and Interactions with Particles*; Onofri, F., Stout, B., Eds.; Aix-Marseille University: Marseille, France, 2014; paper FF-1.
(44) Bohren, C. F.; Huffman, D. R. *Absorption and Scattering of Light by Small Particles*; Wiley: New York, 1983.
(45) Mishchenko, M. I.; Travis, L. D.; Lacis, A. A. *Scattering, Absorption, and Emission of Light by Small Particles*; Cambridge University Press: Cambridge, 2002.
(46) ADDA − Light Scattering Simulator Using the Discrete Dipole Approximation. http://code.google.com/p/a-dda/ (accessed Sep 23, 2015).
(47) Huntemann, M.; Heygster, G.; Hong, G. Discrete Dipole Approximation Simulations on GPUs Using OpenCL − Application on Cloud Ice Particles. *J. Comput. Sci.* **2011**, *2*, 262−271.
(48) Yurkin, M. A.; Hoekstra, A. G. User Manual for the Discrete Dipole Approximation Code ADDA 1.3b4. http://a-dda.googlecode.com/svn/tags/rel_1.3b4/doc/manual.pdf (accessed Sep 23, 2015).
(49) Lyamkina, A. A.; Moshchenko, S. P. Influence of Localized Surface Plasmon in a Lens-Shaped Metal Cluster on the Decay Dynamics of a Point-Dipole Emitter. *J. Quant. Spectrosc. Radiat. Transfer* **2015**, *156*, 12−16.
(50) Todisco, F.; D'Agostino, S.; Esposito, M.; Fernàndez-Domìnguez, A. I.; De Giorgi, M.; Ballarini, D.; Dominici, L.; Tarantini, I.; Cuscunà, M.; Della Sala, F.; Gigli, G.; Sanvitto, D. Exciton-Plasmon Coupling Enhancement via Metal Oxidation. *ACS Nano* **2015**, *9*, 9691−9699.
(51) Doicu, A.; Schuh, R.; Wriedt, T. Scattering by Particles on or near a Plane Surface. In *Light Scattering Reviews 3*; Kokhanovsky, A. A., Ed.; Springer: Berlin, 2008; pp 109−130.

DOI: 10.1021/acs.jpcc.5b09271
J. Phys. Chem. C 2015, 119, 29088−29094

(52) Yurkin, M. A.; Maltsev, V. P.; Hoekstra, A. G. Convergence of the Discrete Dipole Approximation. II. An Extrapolation Technique to Increase the Accuracy. *J. Opt. Soc. Am. A* **2006**, *23*, 2592−2601.
(53) NFM-DS. http://www.scattport.org/index.php/light-scattering-software/t-matrix-codes/list/239-nfm-ds (accessed Sep 23, 2015).
(54) Flatau, P. J.; Draine, B. T. Fast near Field Calculations in the Discrete Dipole Approximation for Regular Rectilinear Grids. *Opt. Express* **2012**, *20*, 1247−1252.
(55) Ayranci, I.; Vaillon, R.; Selcuk, N. Performance of Discrete Dipole Approximation for Prediction of Amplitude and Phase of Electromagnetic Scattering by Particles. *J. Quant. Spectrosc. Radiat. Transfer* **2007**, *103*, 83−101.
(56) Podowitz, D. I.; Liu, C.; Yang, P.; Yurkin, M. A. Comparison of the Pseudo-Spectral Time Domain Method and the Discrete Dipole Approximation for Light Scattering by Ice Spheres. *J. Quant. Spectrosc. Radiat. Transfer* **2014**, *146*, 402−409.

DOI: 10.1021/acs.jpcc.5b09271
J. Phys. Chem. C 2015, 119, 29088−29094